Enhanced Radiation Therapy of Gold Nanoparticles in Liver Cancer

Meili Guo [1], Yuanming Sun [2],* and Xiao-Dong Zhang [2,3],*

[1] Department of Physics, School of Science, Tianjin Chengjian University, Tianjin 300384, China; meiliguo314@163.com

[2] Tianjin Key Laboratory of Molecular Nuclear Medicine, Institute of Radiation Medicine, Chinese Academy of Medical Sciences and Peking Union Medical College, Tianjin 300192, China

[3] Department of Physics and Tianjin Key Laboratory of Low Dimensional Materials Physics and Preparing Technology, Institute of Advanced Materials Physics, School of Science, Tianjin University, Tianjin 300350, China

* Correspondence: sunyuanming@irm-cams.ac.cn (Y.S.); xiaodongzhang@tju.edu.cn (X.-D.Z.); Tel.: +86-22-8568-3045 (Y.S.); +86-22-27404118(X.-D.Z.)

Abstract: Gold nanoparticles (GNPs) were widely used in X-ray imaging and radiation therapy due to strong photoelectric effects and secondary electrons under high energy irradiation. As liver cancer is one of the most common forms of cancer, the use of GNPs could enhance liver cancer radiotherapy. We synthesized polyethylene glycol (PEG)-coated GNPs of two different sizes by chemical reduction reaction. Blood stability, cellular uptake, cytotoxicity and radiation therapy were investigated. A 3–5 nm red shift of SPR caused by interactions between PEG-coated GNPs and plasma indicated their good stability. Cellular uptake assay showed that PEG-coated GNPs would enhance an appreciable uptake. GNPs preferred to combine with blood proteins, and thus induced the formation of 30–50 nm Au-protein corona. GNPs were endocytosed by cytoplasmic vesicles, localized in intracellular region, and presented concentration dependent cell viability. Clonogenic assay illustrated that the PEG-coated GNPs could sensitize two liver cancer cell lines to irradiation.

Keywords: PEG-coated GNPs; cytotoxicity; radiosensitization; liver cancer

1. Introduction

Nanomaterials and nanotechnology have attracted wide attention in biomedicine [1–6]. Owing to their unique optical and electric properties, gold nanoparticles (GNPs) have been wildly used in diverse research areas in recent years [7–10]. Their advantages in size-dependent surface plasmon resonance (SPR), strong X-ray absorption, and easy-surface functionalization make GNPs particularly useful in biosensors, radiation therapy and photothermal therapy [11–18]. GNPs have a great compatibility with biological macromolecules (e.g., amino acids, proteins, and DNA), making them suitable and stable during drug delivery and cancer cell imaging [18–20]. In particular, high X-ray absorption of GNPs makes them applicable to cancer radiation therapy [21].

Cancer radiation therapy is closely related to the capability of cellular uptake of GNPs, which can be determined by its surface chemistry and particle size [22–26]. Bare GNPs are known to be unstable and they tend to aggregate in blood due to high Zeta potential [27]. A surface stabilized coating has been demonstrated to improve the stability of GNPs in blood and induce a higher cellular uptake [28–30]. For example, bare GNPS reportedly formed 150 nm particles that were absorbed by macropinocytosis [31]. In contrast, polyethylene glycol (PEG)-coated GNPs were relatively stable and they were absorbed by endocytosis [32,33]. However, 3.5 nm GNPs containing lysine or poly(L-lysine) were reported to be biocompatible and had no nonimmunogenic effects [34,35], while GNPs coated

with hexadecyl-trimethyl-ammonium bromide were not biocompatible [36]. Besides, the size of GNPs also played an important role in the process of cellular uptake. For instance, 50 nm bare GNPs were found to have highest capability of cellular uptake [37–39], however PEG-coated GNPs of 10~30 nm exhibited a higher inducible effect in uptake [40–45].

Liver cancer (also named as hepatocellular carcinoma) is a common cancer [46] but with a very high fatality rate, almost all patients are dead within a year. The reason of high mortal rate was attributable to hepatitis virus infection. It was reported that about three quarters of patients suffering from liver cancer were found in Southeast Asia including China, Hong Kong, Taiwan, Korea and Japan. Unfortunately, the number of diagnosed patients in the whole world was increasing dramatically, and it will continue to go up over the next few decades. However, liver cancer cells were not sensitive to radiation, and no effective radio-sensitizer has yet been developed for therapeutic treatment. Thus it is really critical to develop an effective and safe method for hepatocellular carcinoma radiation therapy.

In previous work, we investigated the in vivo toxicity and biological applications of GNPs and MoS2 dots in detail [6,30,47–51]. In this study, we will present the therapeutic effect of PEG-coated GNPs using human hepG2 and mouse H22 hepatocellular carcinoma cell line. We found that GNPs had a tendency to aggregate after adding a high concentration of salts and certain biological molecules including nucleic acids and some proteins. Stability of bio-conjugates of GNPs in aqueous solutions is a critical issue in bio-applications. In our study, we found PEG-SH modified GNPs to be more stable compared to other thiol-compounds in aqueous solutions (e.g., cysteine and homocysteine) [52]. We assessed the stability of GNPs in plasma, cellular uptake and their intracellular distribution, cytotoxicity, and radiation therapeutic effect under radiation by ^{137}Cs at doses of 0–4 Gy in two different cell lines. It was illustrated that modifying the surface coating of nanoparticles could achieve low cytotoxicity and high radio-sensitization effect in liver cancer therapy.

2. Materials and Methods

2.1. Fabrication of PEG-Coated GNPs

PEG-coated GNPs of 14.4 and 30.5 nm diameter were used in this study. The particles were fabricated as described by Turkevich [53]. Briefly, 10 mg of HAuCl$_4$·4H$_2$O was dissolved in 100 mL of water and then boiled. After adding 1.3 and 5 mL of 1% sodium citrate solution as a reducing agent, the mixture was boiled for a further 30 min before being allowed to cool to room temperature. Average diameter of GNPs was determined to be 14.4 and 30.5 nm. The prepared GNPs were negatively charged due to the anionic citric acid bound to the surface of GNPs.

To obtain PEG-coated GNPs, 1 mg PEG-SH (Sigma, St. Louis, MO, USA) was added to the solution prepared above and stirred for 1 h. After PEGylation, the solution was centrifuged at 16,000 rpm for 30 min and washed twice using distilled water. Then the PEG-coated GNP solution was stored at 4 °C. Prior to use, the PEG-coated GNP solution was filtered through a 0.22-μm membrane filter.

The morphology, structure and size of GNPs were analyzed by transmission electron microscopy (TEM; Hitachi HF-2000, Hitachi, Tokyo, Japan) at 200 kV. The particles were also characterized by ultraviolet-visible (UV-Vis) spectroscopy (UV-1750. Shimadzu, Kyoto, Japan) to detect the optical absorption from 400 to 700 nm. The slit width of the measurement was 1 nm.

2.2. Blood Plasma Stability Study

Equal volume of a diluted human plasma and PEG-coated GNPs (200 μg/mL) in 14.4 nm or 30.5 nm was mixed together and incubated at 37 °C for 0, 0.5, 1, 2, 6, 12 and 24 h. After incubation, the plasma treated PEG-coated GNPs were studied using UV-Vis spectroscopy to detect the optical absorption from 400 to 700 nm. The slit width of the measurement was 1 nm.

2.3. Cell Culture and Cytotoxicity Assay

Mouse H22 hepatoma cell line and human liver cancer cell line HepG2 were used in all cell culture experiments. These two cell lines were cultured in RPMI-1640 (HyClone) medium supplemented with

10% fetal bovine serum (FBS; Hangzhou Sijiqing, Hangzhou, China), 45 IU/mL streptomycin-penicillin. All cells were maintained at 37 °C in a 5% CO_2 incubator and replenished with fresh medium every 3 days. Cells from passages six to eight were suitable for experiments.

A cell Titer-Glo luminescent cell viability assay, which quantifies metabolically active cells, was performed to determine cytotoxicity of PEG-coated GNPs in two cell lines. Briefly, cells were seeded at an initial density of 3000 cells/100 µL per well in a 96-well plate. After an overnight growth, the cells were replenished with fresh medium and treated with PEG-coated GNPs at different concentrations (0, 12.5, 25, 50, 100, and 200 µg/mL, Au atom concentration), then incubated for 24 h and 48 h. After replenishing with freshly prepared RPMI-1640 medium (100 µL), equal volume of CellTiter-Glo Reagent was added to each well. The solution was mixed on an orbital shaker for 2 min lyses before it was incubated at room temperature in order to obtain stable detection signals. Luminescent signal was measured (Infinite 200. Tecan, Lausanne, Switzerland). Triplicate measurements were obtained for each dosage.

2.4. Cellular Morphology with TEM

In all TEM experiments, HepG2 and H22 cells were each seeded in 6 wells, and cultured for 12 h. These cells were replenished with a medium containing PEG-coated GNPs at a final concentration of 25 µg/mL (Au atom concentration) and incubated at 37 °C with 5% CO_2. After 24 h, cells treated with nanoparticles were trypsinized (HepG2), centrifuged, washed twice with phosphate buffered saline, and collected on copper grids, then analyzed using a field emission high-resolution TEM (Hitachi HF-2000, Hitachi, Tokyo, Japan) at 200 kV.

2.5. Clonogenic Cell Survival Measurement

H22 cells were treated with PEG-GNPs of 14.4 or 30.5 nm diameter at the desired concentration (25 µg/mL, Au atom concentration). After 24 h, these cells were irradiated by ^{137}Cs at the following doses: 0, 1, 2 and 4 Gy, then the culture medium was replaced with fresh one containing 10% FBS. H22 cells were suspended in 0.3% agar and then plated over underlay of 2.0% agar. The medium used in the assay was RPMI-1640 (HyClone) with 10% FBS, penicillin and streptomycin at the concentration of 45 IU/mL. Colonies were counted at day 7.

HepG2 cells were seeded in 6-well and grown for 12 h. PEG-coated GNPs of 14.4 or 30.5 nm diameter in the colloid solution were added to a final concentration of 25 µg/mL (Au atom concentration) and incubated for a further 24 h. Cells were irradiated by ^{137}Cs, the irradiated doses were 0, 1, 2 and 4 Gy. After gamma irradiation, the medium containing colloidal nanoparticles were replenished with freshly prepared medium, and culture media were changed every 3 days. After a two-week incubation, cells were rinsed with phosphate buffered saline containing 2 mL ethanol and stained by crystal violet. Plates were kept in air until dry, then colonies were counted. Each condition was performed in triplicate.

2.6. Statistical Analysis

Data were presented as mean ± standard deviation (SD), unless otherwise specified. A PASW 18.0 software package (SPSS) (IBM, Chicago, IL, USA, 2009 was used in a one-way ANOVA and Student's *t*-test. Difference less than 0.05 ($p < 0.05$) were considered statistically significant.

3. Results and Discussion

3.1. Synthesis and Characterization

Figure 1 shows the UV-Vis spectra of PEG-coated GNPs and GNPs alone. PEG-coated GNPs were obtained through mixing PEG-SH with GNPs and stabilized by sodium citrate. Characteristic SPR of GNPs is shown. Size distribution, aggregation, and surface modified of the particles are indicated

through peak position and width [54]. Compared spectrum between GNPs and PEG-coated GNPs, a slight red shift was observed in the SPR band maxima in modified GNPs group.
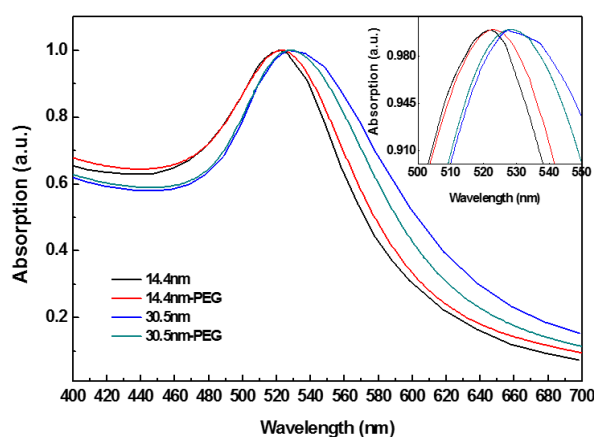
Figure 1. The optical absorption of polyethylene glycol (PEG)-coated gold nanoparticles (GNPs).

PEG-SH contains SH- terminal that can easily form coating through Au-S interaction. The terminal of PEG-SH with a strong hydrophilicity can enhance water-soluble capability of GNPs. The narrow width at half height (~43 nm) indicated that PEG-coated GNPs had a good uniformity. When the concentration of PEG-SH bounded with surface of nanoparticles was low, it made chains of PEG-SH too far to interact with each other, thus the chains formed a "mushroom" configuration through bending and coiling. In contrast, when PEG-SH had a high concentration, the chains were tightly packed and fully extended in solution to form a "brush" structure [55]. In this study we added a concentration close to the saturation ratio (10:1) to increase the likelihood for obtaining a "brush" configuration, and then a certain thickness of PEG layer formed in the GNPs' surface, which increased dispersion and biocompatibility of the particles.

Figure 2 displays the transmission electron micrographs and size distribution of GNPs. Using these transmission electron micrographs, an average diameter of ~14.4 nm was measured for the smaller sized spherical particles and ~30.5 nm for the larger particles. The size distribution was found generally to be <20% of the standard deviation. PEG-coated GNPs were used in all the following experiments.
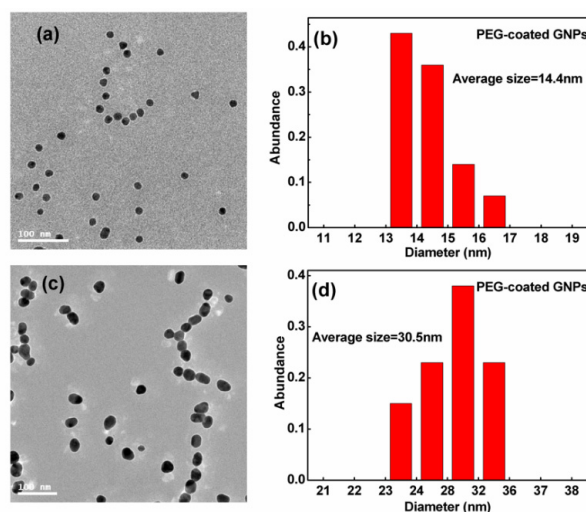
Figure 2. (**a**,**c**) Transmission electron microscopy (TEM) images of 14.4 and 30.5 nm GNPs; (**b**,**d**) corresponding distribution of 14.4 and 30.5 nm GNPs.

3.2. Blood Plasma Stability

To determine stability of GNPs in the solution containing serum and address how culture medium might influence particle aggregation, we treated plasma with PEG-coated GNPs. Figure 3a shows the time-dependent optical absorption spectrum of 14.4 and 30.5 nm PEG-coated GNPs incubated in plasma. A red shift in the absorption peak was observed in the two different sized PEG-coated GNPs due to slight aggregation of particles bound to a range of proteins. The peak was related to the structure and optical properties of nanoparticles, indicating that nanoparticles combined with the plasma proteins to form large compounds during this period. Figure 3b also shows that the intensity of absorption peak was significantly reduced as time increased, but red shift of SPR and change of half peak width were slight. All of these data indicated a higher number of protein immobilised nanoparticles would reduce the absorption intensity.
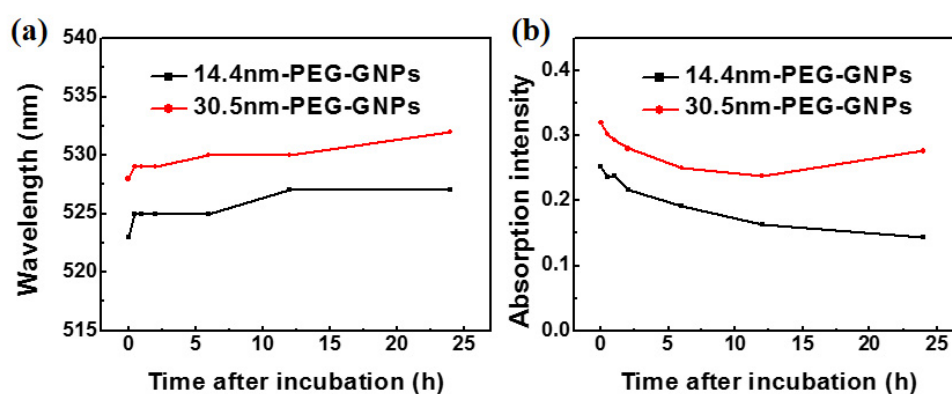

Figure 3. Time-dependent surface plasmon resonance (SPR) peak (**a**) and intensity (**b**) of 14.4 and 30.5 nm PEG-coated GNPs on blood plasma.

Stability of nanoparticles in biomedical applications depends on particle bio-distribution and clearance in the body. They are related to many features of the particles themselves, including size and particle surface charge valence. Blood protein coated nanoparticles played an important role in toxicity [56,57]. The characteristics of these proteins, which form a parcel layer, may affect the biological response of nanoparticles, including the impact on the uptake and accumulation in the organs [49].

3.3. Distribution of PEG-Coated GNPs in Cells

Surface modification of the GNPs is expected to affect endocytosis and cellular transportation of GNPs in cells. Representative transmission electron micrographs of intracellular uptake of PEG-coated GNPs of 14.4 nm and 30.5 nm diameter by HepG2 and H22 cells during a 24 h treatment are shown in Figure 4. These micrographs gave a microscopic insight of the distribution of nanoparticles. The figure showed that PEG-coated GNPs were distributed in the cytoplasm and observed in the intracellular region. We further found a cellular uptake of 10^3 nanoparticles per cell in HepG2 and H22 cells, as shown in Figure 5. Moreover, there was a 66% cellular uptake for the 30.4 nm and 62% for 14.4 nm GNPs in HepG2 cell, respectively. These findings are consistent with recent reports that 30 nm PEG-coated GNPs presented higher potential of cellular uptake [18,23,32,58,59]. The transmission electron micrographs obtained for PEG-coated GNPs in H22 and HepG2 cell line are shown in Figure 6a,b, respectively. The particles were wrapped in structure similar to vesicles. In the transmission electron micrographs, the nanoparticles with size of ~15 nm and 30–50 nm was observed, most likely because of the formation of a large size corona following the interaction between GNPs and proteins, as illustrated by the schematic in Figure 6c. This observation is in good agreement with that of blood plasma stability in Figure 3.
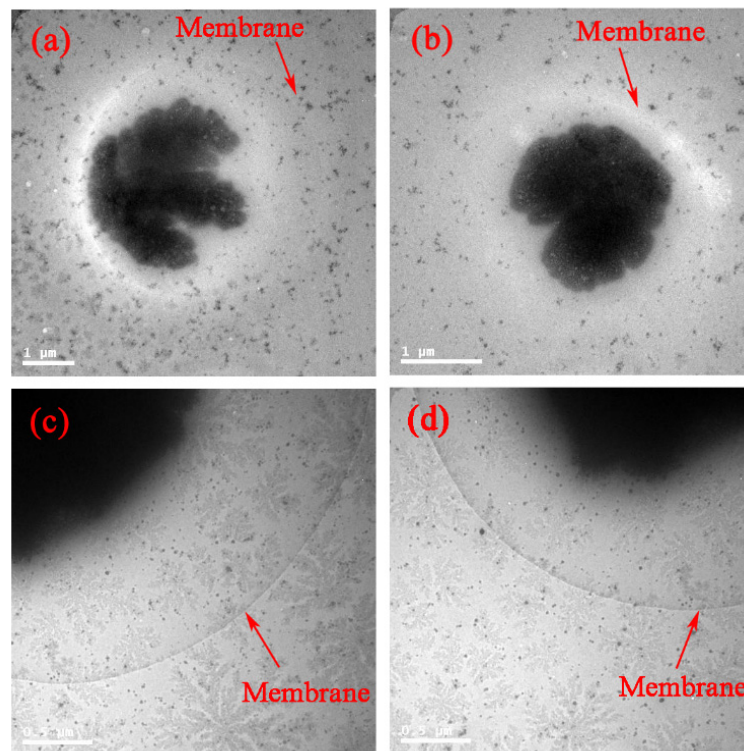
Figure 4. In vitro bio-distribution and TEM images of 14.4 and 30.5 nm PEG-coated GNPs in H22 (**a**,**c**) and HepG2 (**b**,**d**) cell.
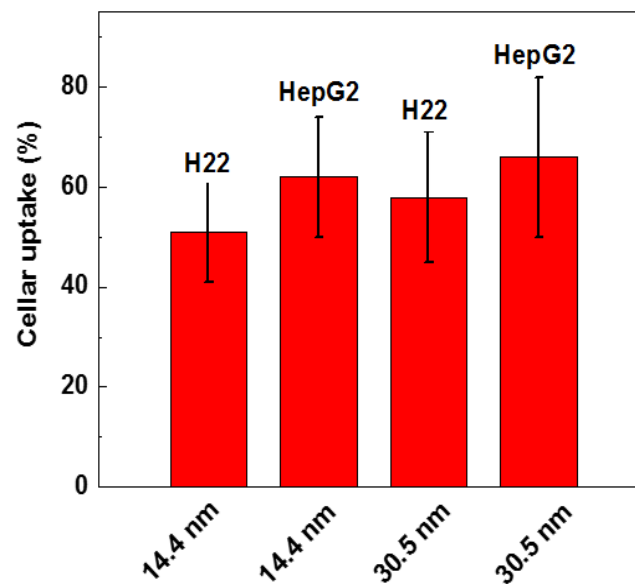
Figure 5. Cellular uptake of 14.4 and 30.5 nm PEG-coated GNPs in H22 and HepG2 cells.

We added PEG-coated GNPs to cells and studied their response by TEM. The charges on the surface of GNPs changed from negative to positive because of PEG-SH modifying, which made them easily interact with cells that carried negative charges on the surface, and enhanced the binding between nanoparticles and cells. When nanoparticles carrying positive charges were added to cells, they were electrostatically attracted to the membrane surface carrying negative charges. Endocytosis played a critical role in the interaction of nanoparticles with cells. GNPs modified with different agents would play different roles in endocytosis [60].
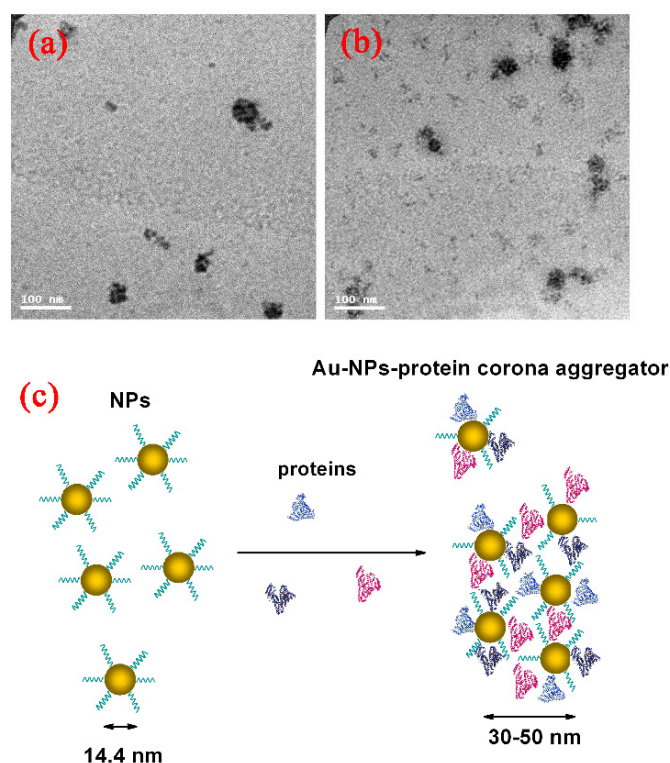
Figure 6. Direct observation of Au-protein corona aggregator by TEM imaging in H22 (**a**); HepG2 cells (**b**); and blood dynamic (**c**) of GNPs in physiological environment.

3.4. Cytotoxicity of PEG-Coated GNPs

To assess cytotoxicity of nanoparticles, we performed a CellTiter-Glo luminescent cell viability assay, which quantitatively measures the concentration of ATP that is related to the number of metabolically active cells in a culture. The amount of ATP was positively correlated to cells present in culture. Figure 7 shows the results of cytotoxicity in H22 and HepG2 cells after 24 h treatment with PEG-coated GNPs of 14.4 nm or 30.5 nm at various concentrations (0–200 μg/mL, Au atom concentration). The 14.4 nm particles showed 58% cell viability values that higher than 42% of 30.5 nm particles in HepG2 cells after 24 h at the dose of 100 μg/mL. Viability of H22 cells exposed to control group decreased by 15% after being treated with 12.5 μg/mL GNPs, and 75% after being treated with 200 μg/mL. Cell viability of HepG2 cells was 95% and 100% when treated with 12.5 μg/mL 14.4 nm and 30.5 nm GNPs, respectively, and decreased to 27% and 22% respectively at the highest concentration of 200 μg/mL, indicating that the toxicity would increase when the concentration went up to a higher value.

In the cell viability assay, both PEG-coated GNPs of 14.4 nm and 30.5 nm diameter showed anti-proliferative effects in a concentration dependent manner, and PEG-coated GNPs of 14.4 nm was in general significantly ($p < 0.05$) less toxic to the cells than 30.5 nm. In addition, 25 μg/mL of PEG-coated GNPs of 14.4 nm or 30.5 nm became slightly more toxicy after 24 h in culture (Figure 7). These results were consistent with the phenomenon of particles distribution in Figure 4. Moreover, PEG-coated GNPs of 30.5 nm were about 10%–20% more abundant than those of 14.4 nm in the cytoplasm, which could have an influence on cell viability. These two GNPs were used for the radio-sensitization experiments in H22 and HepG2 cells to evaluate their ability in sensitizing the cells to radiation.
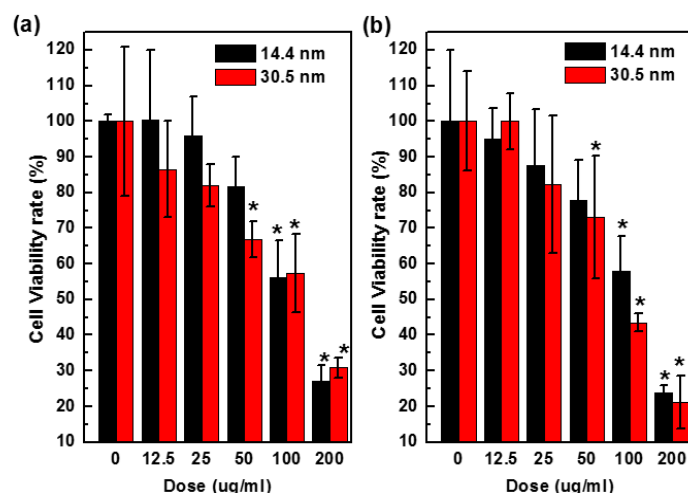
Figure 7. Concentration dependent toxicity in vitro H22 (**a**) and HepG2 cells (**b**) treated with 14.4 or 30.5 nm PEG-coated GNPs after 24 h.

3.5. Enhanced Radiotherapy

A clonogenic cell survival assay was used to determine the radio-sensitization effect between the two nanoparticles in H22 and HepG2 cells, and the results are shown in Figure 8a,b, respectively. After treated with or without PEG-coated GNPs for 24 h, both cell lines were radiated under 0, 1, 2, and 4 Gy by ^{137}Cs. Under 1 Gy of the radiation, the survival fraction of control group, the 14.4 nm group, and the 30.5 nm group was 95.00%, 49.46% and 76.61% in H22 cells respectively; while in HepG2 cells was 90%, 49.92% and 50.25% respectively. When exposed to 2 Gy, the survival fraction of control group, 14.4 nm group, and 30.5 nm group were 47.98%, 31.42% and 33.58% in H22 cells respectively; and 56.96%, 28.04% and 33.75% in HepG2 cells respectively. In previous work, the sensitizer enhancement ratios were 1.16–1.66, which depended on the particles size, cellar line, surface coating and radiation energy (Table 1). In our work, sensitizer enhancement ratios were about 1.2–1.3 according to previous calculation methods [18]. These data illustrated that no matter whether they were radiated alone or radiated and treated with nanoparticles, the cell colony formation rates were low, indicating that the nanoparticles and radiation can inhibit tumor cell proliferation.

Figure 8 showed how PEG-coated GNPs affected cell survival fraction under different radiation doses. Enhanced effect of nanoparticles modified with PEG-SH was observed on inhibition of the cell viability by radiation. Under identical concentration of PEG-coated GNPs, cells showed decreased survival percentages when radiation doses increased.
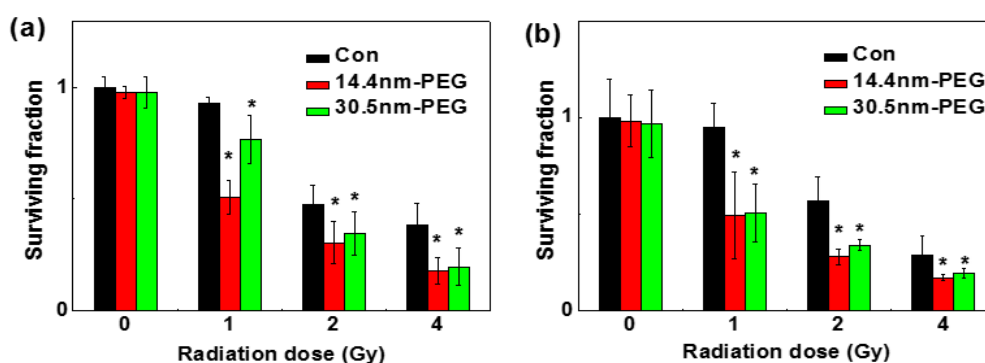
Figure 8. Cloning formations in H22 (**a**) and HepG2 cells (**b**) after treated with 0.05 mM 14.4 or 30.5 nm PEG-coated GNPs.

Table 1. Summary of the enhanced cancer radiation of gold nanoparticles.

Materials	Size	Surface	Cell	Sensitizer Enhancement Ratios
Gold NPs	nm	Bare	MDA-MB-231	1.16–1.41 [61]
Gold NPs	14 nm, 74 nm	Bare	Hela	1.17–1.66 [62]
Gold NPs	4.8 nm, 46.6 nm	PEG	HeLa	1.41 [18]
Gold NPs	1.9 nm	Bare	MDA-MB-231	1.18, 1.24 [63]
Au clusters	2.1 nm	GSH	Hela	1.21, 1.3 [28]
Gold NPs	14.4 nm, 30.5 nm	PEG	H22, HepG2	1.2–1.3 (This work)

4. Conclusions

In this study, we studied the radiation enhancement effects in liver cancer cell lines by using 14.4 and 30.5 nm PEG-coated GNPs. Our results showed that PEG-coated GNPs were stable in blood. The in vitro bio-distribution assay showed PEG-coated GNPs had higher distribution in cancer cells, about 10^3 NPs were found in one cell. TEM direct observation illustrated that PEG-coated GNPs hybridized with blood proteins and formed a 30–50 nm Au-protein corona. Further, these GNPs were of low toxicity at the concentration of 10^{-4} M. In vitro radiation treatment showed GNPs significantly enhanced the irradiation effect and decreased the survival of two types of liver cancer cells. Thus, PEG-coated GNPs can be considered as a potential agent in liver cancer radiation therapy.

Author Contributions: X.-D.Z and Y.S. conceived and designed the experiments; X.-D.Z., M.G. and Y.S. performed the experiments; M.G., X.-D.Z and Y.S. analyzed the data; X.-D.Z contributed reagents/materials/analysis tools; M.G and X.D.Z. wrote the paper." Authorship must be limited to those who have contributed substantially to the work reported.

Conflicts of Interest: The authors declare no conflict of interest.

References

1. Koseki, Y.; Ikuta, Y.; Kamishima, T.; Onodera, T.; Oikawa, H.; Kasai, H. Drug Release is Determined by the Chain Length of Fatty Acid-Conjugated Anticancer Agent as One Component of the Nano-prodrugs. *Bull. Chem. Soc. Jpn.* **2016**, *89*, 540–545. [CrossRef]

2. Lim, E.-K.; Kim, T.; Paik, S.; Haam, S.; Huh, Y.-M.; Lee, K. Nanomaterials for theranostics: Recent advances and future challenges. *Chem. Rev.* **2014**, *115*, 327–394. [CrossRef] [PubMed]

3. Ariga, K.; Minami, K.; Ebara, M.; Nakanishi, J. What are the emerging concepts and challenges in NANO? Nanoarchitectonics, hand-operating nanotechnology and mechanobiology. *Polym. J.* **2016**, *48*, 371–389.

4. Wicki, A.; Witzigmann, D.; Balasubramanian, V.; Huwyler, J. Nanomedicine in cancer therapy: Challenges, opportunities, and clinical applications. *J. Control. Release* **2015**, *200*, 138–157. [CrossRef] [PubMed]

5. Yamamoto, E.; Kuroda, K. Colloidal Mesoporous Silica Nanoparticles. *Bull. Chem. Soc. Jpn.* **2016**, *89*, 501–539. [CrossRef]

6. Zhang, X.-D.; Zhang, J.; Wang, J.; Yang, J.; Chen, J.; Shen, X.; Deng, J.; Deng, D.; Long, W.; Sun, Y.-M. Highly catalytic nanodots with renal clearance for radiation protection. *ACS Nano* **2016**, *10*, 4511–4519. [CrossRef] [PubMed]

7. Xie, J.; Zheng, Y.; Ying, J.Y. Protein-directed synthesis of highly fluorescent gold nanoclusters. *J. Am. Chem. Soc.* **2009**, *131*, 888–889. [CrossRef] [PubMed]

8. Luo, Z.; Yuan, X.; Yu, Y.; Zhang, Q.; Leong, D.T.; Lee, J.Y.; Xie, J. From aggregation-induced emission of Au(I)–thiolate complexes to ultrabright Au(0)@Au(I)–thiolate core–shell nanoclusters. *J. Am. Chem. Soc.* **2012**, *134*, 16662–16670. [CrossRef] [PubMed]

9. Zhang, X.-D.; Guo, M.-L.; Wu, D.; Liu, P.-X.; Sun, Y.-M.; Zhang, L.-A.; She, Y.; Liu, Q.-F.; Fan, F.-Y. First-principles investigation of Ag-doped gold nanoclusters. *Int. J. Mol. Sci.* **2011**, *12*, 2972–2981. [CrossRef] [PubMed]

10. Zhang, X.; Guo, M. Electronic structure and optical transitions of $Au_{20-x}Cu_x$ nanoclusters. *J. Nanosci. Nanotechnol.* **2010**, *10*, 7192–7195. [CrossRef]

11. Huang, X.; El-Sayed, I.H.; Qian, W.; El-Sayed, M.A. Cancer cell imaging and photothermal therapy in the near-infrared region by using gold nanorods. *J. Am. Chem. Soc.* **2006**, *128*, 2115–2120. [CrossRef] [PubMed]

12. Hainfeld, J.F.; Slatkin, D.N.; Smilowitz, H.M. The use of gold nanoparticles to enhance radiotherapy in mice. *Phys. Med. Biol.* **2004**, *49*, N309. [CrossRef] [PubMed]

13. Zhang, X.-D.; Wu, D.; Shen, X.; Liu, P.-X.; Yang, N.; Zhao, B.; Zhang, H.; Sun, Y.-M.; Zhang, L.-A.; Fan, F.-Y. Size-dependent in vivo toxicity of PEG-coated gold nanoparticles. *Int. J. Nanomed.* **2011**, *6*, 2071–2081. [CrossRef] [PubMed]

14. Kunjachan, S.; Detappe, A.; Kumar, R.; Ireland, T.; Cameron, L.; Biancur, D.E.; Motto-Ros, V.; Sancey, L.; Sridhar, S.; Makrigiorgos, G.M. Nanoparticle mediated tumor vascular disruption: A novel strategy in radiation therapy. *Nano Lett.* **2015**, *15*, 7488–7496. [CrossRef] [PubMed]

15. Wolfe, T.; Chatterjee, D.; Lee, J.; Grant, J.D.; Bhattarai, S.; Tailor, R.; Goodrich, G.; Nicolucci, P.; Krishnan, S. Targeted gold nanoparticles enhance sensitization of prostate tumors to megavoltage radiation therapy in vivo. *Nanomed NBM* **2015**, *11*, 1277–1283. [CrossRef] [PubMed]

16. Wu, P.; Onodera, Y.; Ichikawa, Y.; Watanabe, Y.; Qian, W.; Hashimoto, T.; Shirato, H.; Nam, J. Gold Nanoparticles With RGD Peptide in Radiation Therapy Suppress the Invasion Activity of Breast Cancer Cells. *Int. J. Radiat. Oncol. Biol. Phys.* **2016**, *96*, E574. [CrossRef]

17. Zhang, P.; Qiao, Y.; Xia, J.; Guan, J.; Ma, L.; Su, M. Enhanced radiation therapy with multilayer microdisks containing radiosensitizing gold nanoparticles. *ACS Appl. Mater. Interfaces* **2015**, *7*, 4518–4524. [CrossRef] [PubMed]

18. Zhang, X.-D.; Wu, D.; Shen, X.; Chen, J.; Sun, Y.-M.; Liu, P.-X.; Liang, X.-J. Size-dependent radiosensitization of PEG-coated gold nanoparticles for cancer radiation therapy. *Biomaterials* **2012**, *33*, 6408–6419. [CrossRef] [PubMed]

19. Kim, D.; Park, S.; Lee, J.H.; Jeong, Y.Y.; Jon, S. Antibiofouling polymer-coated gold nanoparticles as a contrast agent for in vivo X-ray computed tomography imaging. *J. Am. Chem. Soc.* **2007**, *129*, 7661–7665. [CrossRef] [PubMed]

20. Alric, C.; Taleb, J.; Duc, G.L.; Mandon, C.; Billotey, C.; Meur-Herland, A.L.; Brochard, T.; Vocanson, F.; Janier, M.; Perriat, P. Gadolinium chelate coated gold nanoparticles as contrast agents for both X-ray computed tomography and magnetic resonance imaging. *J. Am. Chem. Soc.* **2008**, *130*, 5908–5915. [CrossRef] [PubMed]

21. Zhang, X.-D.; Guo, M.-L.; Wu, H.-Y.; Sun, Y.-M.; Ding, Y.-Q.; Feng, X.; Zhang, L.-A. Irradiation stability and cytotoxicity of gold nanoparticles for radiotherapy. *Int. J. Nanomed.* **2009**, *4*, 165–173. [CrossRef]

22. Albanese, A.; Tang, P.S.; Chan, W.C. The effect of nanoparticle size, shape, and surface chemistry on biological systems. *Annu. Rev. Biomed. Eng.* **2012**, *14*, 1–16. [CrossRef] [PubMed]

23. Cho, E.C.; Zhang, Q.; Xia, Y. The effect of sedimentation and diffusion on cellular uptake of gold nanoparticles. *Nat. Nanotechnol.* **2011**, *6*, 385–391. [CrossRef] [PubMed]

24. Wang, J.-Y.; Chen, J.; Yang, J.; Wang, H.; Shen, X.; Sun, Y.-M.; Guo, M.; Zhang, X.-D. Effects of surface charges of gold nanoclusters on long-term in vivo biodistribution, toxicity, and cancer radiation therapy. *Int. J. Nanomed.* **2016**, *11*, 3475.

25. Wang, C.; Sun, A.; Qiao, Y.; Zhang, P.; Ma, L.; Su, M. Cationic surface modification of gold nanoparticles for enhanced cellular uptake and X-ray radiation therapy. *J. Mater. Chem. B* **2015**, *3*, 7372–7376. [CrossRef] [PubMed]

26. Zhang, X.-D.; Wu, D.; Shen, X.; Liu, P.-X.; Fan, F.-Y.; Fan, S.-J. In vivo renal clearance, biodistribution, toxicity of gold nanoclusters. *Biomaterials* **2012**, *33*, 4628–4638. [CrossRef] [PubMed]

27. Cedervall, T.; Lynch, I.; Lindman, S.; Berggård, T.; Thulin, E.; Nilsson, H.; Dawson, K.A.; Linse, S. Understanding the nanoparticle–protein corona using methods to quantify exchange rates and affinities of proteins for nanoparticles. *Proc. Natl. Acad. Sci. USA* **2007**, *104*, 2050–2055. [CrossRef] [PubMed]

28. Zhang, X.D.; Chen, J.; Luo, Z.; Wu, D.; Shen, X.; Song, S.S.; Sun, Y.M.; Liu, P.X.; Zhao, J.; Huo, S. Enhanced Tumor Accumulation of Sub-2 nm Gold Nanoclusters for Cancer Radiation Therapy. *Adv. Healthc. Mater.* **2014**, *3*, 133–141. [CrossRef] [PubMed]

29. Zhang, X.-D.; Luo, Z.; Chen, J.; Song, S.; Yuan, X.; Shen, X.; Wang, H.; Sun, Y.; Gao, K.; Zhang, L. Ultrasmall glutathione-protected gold nanoclusters as next generation radiotherapy sensitizers with high tumor uptake and high renal clearance. *Sci. Rep.* **2015**, *5*, 8669. [CrossRef] [PubMed]

30. Zhang, X.D.; Luo, Z.; Chen, J.; Shen, X.; Song, S.; Sun, Y.; Fan, S.; Fan, F.; Leong, D.T.; Xie, J. Ultrasmall Au$_{10-12}$ (SG)$_{10-12}$ nanomolecules for high tumor specificity and cancer radiotherapy. *Adv. Mater.* **2014**, *26*, 4565–4568. [CrossRef] [PubMed]

31. Lin, W.; Insley, T.; Tuttle, M.D.; Zhu, L.; Berthold, D.A.; Kral, P.; Rienstra, C.M.; Murphy, C.J. Control of protein orientation on gold nanoparticles. *J. Phys. Chem. C* **2015**, *119*, 21035–21043. [CrossRef]

32. Brandenberger, C.; Mühlfeld, C.; Ali, Z.; Lenz, A.G.; Schmid, O.; Parak, W.J.; Gehr, P.; Rothen-Rutishauser, B. Quantitative evaluation of cellular uptake and trafficking of plain and polyethylene glycol-coated gold nanoparticles. *Small* **2010**, *6*, 1669–1678. [CrossRef] [PubMed]

33. Alkilany, A.M.; Nagaria, P.K.; Hexel, C.R.; Shaw, T.J.; Murphy, C.J.; Wyatt, M.D. Cellular uptake and cytotoxicity of gold nanorods: Molecular origin of cytotoxicity and surface effects. *Small* **2009**, *5*, 701–708. [CrossRef] [PubMed]

34. Shukla, R.; Bansal, V.; Chaudhary, M.; Basu, A.; Bhonde, R.R.; Sastry, M. Biocompatibility of gold nanoparticles and their endocytotic fate inside the cellular compartment: A microscopic overview. *Langmuir* **2005**, *21*, 10644–10654. [CrossRef] [PubMed]

35. Connor, E.E.; Mwamuka, J.; Gole, A.; Murphy, C.J.; Wyatt, M.D. Gold nanoparticles are taken up by human cells but do not cause acute cytotoxicity. *Small* **2005**, *1*, 325–327. [CrossRef] [PubMed]

36. Wang, S.; Lu, W.; Tovmachenko, O.; Rai, U.S.; Yu, H.; Ray, P.C. Challenge in understanding size and shape dependent toxicity of gold nanomaterials in human skin keratinocytes. *Chem. Phys. Lett.* **2008**, *463*, 145–149. [CrossRef] [PubMed]

37. Chithrani, B.D.; Ghazani, A.A.; Chan, W.C. Determining the size and shape dependence of gold nanoparticle uptake into mammalian cells. *Nano Lett.* **2006**, *6*, 662–668. [CrossRef] [PubMed]

38. Chithrani, B.D.; Chan, W.C. Elucidating the mechanism of cellular uptake and removal of protein-coated gold nanoparticles of different sizes and shapes. *Nano Lett.* **2007**, *7*, 1542–1550. [CrossRef] [PubMed]

39. Huo, S.; Ma, H.; Huang, K.; Liu, J.; Wei, T.; Jin, S.; Zhang, J.; He, S.; Liang, X.-J. Superior penetration and retention behavior of 50 nm gold nanoparticles in tumors. *Cancer Res.* **2013**, *73*, 319–330. [CrossRef] [PubMed]

40. Yen, H.J.; Hsu, S.; Tsai, C.L. Cytotoxicity and immunological response of gold and silver nanoparticles of different sizes. *Small* **2009**, *5*, 1553–1561. [CrossRef] [PubMed]

41. Soenen, S.J.; Manshian, B.; Montenegro, J.M.; Amin, F.; Meermann, B.; Thiron, T.; Cornelissen, M.; Vanhaecke, F.; Doak, S.; Parak, W.J. The Cytotoxic Effects of Gold Nanoparticles: A Multiparametric Study. *ACS Nano* **2012**, *6*, 5767–5783. [CrossRef] [PubMed]

42. Cho, W.S.; Kim, S.; Han, B.S.; Son, W.C.; Jeong, J. Comparison of gene expression profiles in mice liver following intravenous injection of 4 and 100nm-sized PEG-coated gold nanoparticles. *Toxic. Lett.* **2009**, *191*, 96–102. [CrossRef] [PubMed]

43. Cho, W.S.; Cho, M.; Jeong, J.; Choi, M.; Cho, H.Y.; Han, B.S.; Kim, S.H.; Kim, H.O.; Lim, Y.T.; Chung, B.H. Acute toxicity and pharmacokinetics of 13 nm-sized PEG-coated gold nanoparticles. *Toxicol. Appl. Pharm.* **2009**, *236*, 16–24. [CrossRef] [PubMed]

44. Zhang, G.; Yang, Z.; Lu, W.; Zhang, R.; Huang, Q.; Tian, M.; Li, L.; Liang, D.; Li, C. Influence of anchoring ligands and particle size on the colloidal stability and in vivo biodistribution of polyethylene glycol-coated gold nanoparticles in tumor-xenografted mice. *Biomaterials* **2009**, *30*, 1928–1936. [CrossRef] [PubMed]

45. Lipka, J.; Semmler-Behnke, M.; Sperling, R.A.; Wenk, A.; Takenaka, S.; Schleh, C.; Kissel, T.; Parak, W.J.; Kreyling, W.G. Biodistribution of PEG-modified gold nanoparticles following intratracheal instillation and intravenous injection. *Biomaterials* **2010**, *31*, 6574–6581. [CrossRef] [PubMed]

46. Okuda, K.; Ohtsuki, T.; Obata, H.; Tomimatsu, M.; Okazaki, N.; Hasegawa, H.; Nakajima, Y.; Ohnishi, K. Natural history of hepatocellular carcinoma and prognosis in relation to treatment study of 850 patients. *Cancer* **1985**, *56*, 918–928. [CrossRef]

47. Zhang, X.D.; Wang, H.; Antaris, A.L.; Li, L.; Diao, S.; Ma, R.; Nguyen, A.; Hong, G.; Ma, Z.; Wang, J. Traumatic brain injury imaging in the second near-infrared window with a molecular fluorophore. *Adv. Mater.* **2016**, *28*, 6872–6879. [CrossRef] [PubMed]

48.　Zhang, X.D.; Chen, J.; Min, Y.; Park, G.B.; Shen, X.; Song, S.S.; Sun, Y.M.; Wang, H.; Long, W.; Xie, J. Metabolizable Bi_2Se_3 nanoplates: Biodistribution, toxicity, and uses for cancer radiation therapy and imaging. *Adv. Funct. Mater.* **2014**, *24*, 1718–1729. [CrossRef]

49.　Zhang, X.-D.; Wu, H.-Y.; Wu, D.; Wang, Y.-Y.; Chang, J.-H.; Zhai, Z.-B.; Meng, A.-M.; Liu, P.-X.; Zhang, L.-A.; Fan, F.-Y. Toxicologic effects of gold nanoparticles in vivo by different administration routes. *Int. J. Nanomed.* **2010**, *5*, 771–781. [CrossRef] [PubMed]

50.　Wu, D.; Zhang, X.-D.; Liu, P.-X.; Zhang, L.-A.; Fan, F.-Y.; Guo, M.-L. Gold nanostructure: Fabrication, surface modification, targeting imaging, and enhanced radiotherapy. *Curr. Nanosci.* **2011**, *7*, 110–118. [CrossRef]

51.　Chen, J.; Wang, H.; Long, W.; Shen, X.; Wu, D.; Song, S.; Sun, Y.; Liu, P.; Fan, S.; Fan, F. Sex differences in the toxicity of polyethylene glycol-coated gold nanoparticles in mice. *Int. J. Nanomed.* **2013**, *8*, 2409–2419.

52.　Gao, J.; Huang, X.; Liu, H.; Zan, F.; Ren, J. Colloidal Stability of Gold Nanoparticles Modified with Thiol Compounds, Bioconjugation and Application in Cancer Cell Imaging. *Langmuir* **2012**, *28*, 4464–4471. [CrossRef] [PubMed]

53.　Turkevich, J.; Stevenson, P.C.; Hillier, J. A study of the nucleation and growth processes in the synthesis of colloidal gold. *Discuss. Faraday Soc.* **1951**, *11*, 55–75. [CrossRef]

54.　Daniel, M.C.; Astruc, D. Gold Nanoparticles: Assembly, Supramolecular Chemistry, Quantum-Size-Related Properties, and Applications toward Biology, Catalysis, and Nanotechnology. *Chem. Rev.* **2004**, *104*, 293–346. [CrossRef] [PubMed]

55.　Wu, C.; Guo, H.; Hu, J. Stability of Thiolated PEG 5000-Coated Gold Colloids: From DLVO Stability to Steric Stability. *Acta Chim. Sin.* **2009**, *67*, 1621–1625.

56.　Dobrovolskaia, M.A.; Patri, A.K.; Zheng, J.; Clogston, J.D.; Ayub, N.; Aggarwal, P.; Neun, B.W.; Hall, J.B.; McNeil, S.E. Interaction of colloidal gold nanoparticles with human blood: Effects on particle size and analysis of plasma protein binding profiles. *Nanomed. NBM* **2009**, *5*, 106–117. [CrossRef] [PubMed]

57.　Lacerda, S.H.D.P.; Park, J.J.; Meuse, C.; Pristinski, D.; Becker, M.L.; Karim, A.; Douglas, J.F. Interaction of gold nanoparticles with common human blood proteins. *ACS Nano* **2009**, *4*, 365–379. [CrossRef] [PubMed]

58.　Nativo, P.; Prior, I.A.; Brust, M. Uptake and intracellular fate of surface-modified gold nanoparticles. *ACS Nano* **2008**, *2*, 1639–1644. [CrossRef] [PubMed]

59.　Zhu, Z.J.; Posati, T.; Moyano, D.F.; Tang, R.; Yan, B.; Vachet, R.W.; Rotello, V.M. The interplay of monolayer structure and serum protein interactions on the cellular uptake of gold nanoparticles. *Small* **2012**, *8*, 2659–2663. [CrossRef] [PubMed]

60.　Kong, T.; Zeng, J.; Wang, X.; Yang, X.; Yang, J.; McQuarrie, S.; McEwan, A.; Roa, W.; Chen, J.; Xing, J.Z. Enhancement of radiation cytotoxicity in breast-cancer cells by localized attachment of gold nanoparticles. *Small* **2008**, *4*, 1537–1543. [CrossRef] [PubMed]

61.　Jain, S.; Coulter, J.A.; Hounsell, A.R.; Butterworth, K.T.; McMahon, S.J.; Hyland, W.B.; Muir, M.F.; Dickson, G.R.; Prise, K.M.; Currell, F.J. Cell-specific radiosensitization by gold nanoparticles at megavoltage radiation energies. *Int. J. Radiat. Oncol. Biol. Phys.* **2011**, *79*, 531–539. [CrossRef] [PubMed]

62.　Chithrani, D.B.; Jelveh, S.; Jalali, F.; van Prooijen, M.; Allen, C.; Bristow, R.G.; Hill, R.P.; Jaffray, D.A. Gold nanoparticles as radiation sensitizers in cancer therapy. *Radiat. Res.* **2010**, *173*, 719–728. [CrossRef] [PubMed]

63.　McMahon, S.J.; Hyland, W.B.; Muir, M.F.; Coulter, J.A.; Jain, S.; Butterworth, K.T.; Schettino, G.; Dickson, G.R.; Hounsell, A.R.; O'Sullivan, J.M. Nanodosimetric effects of gold nanoparticles in megavoltage radiation therapy. *Radiother. Oncol.* **2011**, *100*, 412–416. [CrossRef] [PubMed]